

Warm Season Afternoon Thunderstorm Characteristics under Weak Synoptic-Scale Forcing over Taiwan Island

Pin-Fang Lin^{1,2}, Pao-Liang Chang¹, Ben Jong-Dao Jou²
Meteorological Satellite Center, Central Weather Bureau¹
Department of Atmospheric Sciences, National Taiwan University²

Abstract

By using radar reflectivity and lightning data, the characteristics of spatial and temporal distributions of thunderstorms in Taiwan, in the absence of significant weather systems, were analyzed and documented in this study covering the warm seasons (May–October) from 2005 to 2008. Storms activities were found strongly depending on geography and local circulations, and the most frequent of storms activities was during the periods in afternoon especially during 1500–1600 local solar time (LST). Frequent afternoon thunderstorms were confined primarily to narrow areas on the slopes of mountain ranges, and the movement of the thunderstorms was closely related to the orientations of the mountain ranges in northern and southern Taiwan. Significant diurnal variations were also found in surface wind, temperature, and dew-point temperature on days with and without afternoon thunderstorms (TSA and non-TSA days) defined with reflectivity and lightning data.

1. Introduction

The purposes of this study are to investigate the characteristics of thunderstorms by using various datasets (especially radar data), and the preconvective environments associated with the occurrences of afternoon thunderstorms in the warm seasons (May–October) from 2005 to 2008 in Taiwan. Thunderstorms climatology based on reflectivity and lightning fields have been investigated to improve the accuracy of forecasting the timing and location of thunderstorms (Saxen et al. 2008).

Taiwan, a mountainous island, is characterized with the Central Mountain Range (CMR). Mountains not only generate local circulations but also interact with large-scale low-level winds to produce localized rain showers (Akaeda et al. 1995). The sea–land breeze and anabatic–katabatic flows are important in moistening the boundary layer and provide favorable conditions for the initiation of afternoon thunderstorms (Chen and Li 1995). During the summer months in Taiwan, the convection triggered by relatively few disturbances embedded in the environmental flow, which results in the most significant daytime/nighttime contrast in rainfall occurrences (Kerns et al. 2009).

Jou (1994) found that thunderstorms in northern Taiwan initiated in the mountain peak area and propagated down the terrain slope and brought heavy rain to the basin and plain areas. Outflow boundaries from pre-existing thunderstorms and sea breeze, combining with orographic effects such as upslope flow, can subsequently enhance convective activity (Wilson and Schreiber 1986). As a result, maximum storm activities during afternoon hours in Taiwan tended to occur along the windward slopes of the inner mountains

rather than at higher elevations farther inland (Lin and Kuo 1996; Chen et al. 2001).

2. Data and methodology

In order to assure that the selected cases can well present the impacts of local geographic factors, some factors including the influence of synoptic-scale perturbations, rainfall events affected by fronts, tropical cyclones, etc., were eliminated according to daily weather maps and weather outlooks issued by the CWB. Accordingly, 277 days in the absence of synoptic-scale weather systems (henceforth referred to as undisturbed days) out of a total 736 for the four warm seasons were selected.

On undisturbed days, rain gauge data are used to examine the spatial distribution and the diurnal rainfall cycle, and reflectivity climatology data to investigate the spatial and temporal variations associated with the rainfall regions. Lightning climatology is also utilized to study its relationship with reflectivity. Further, surface station data and radiosonde observations at Panchiao are respectively used to analyze the variations in local-circulation characteristics and large-scale atmospheric conditions favorable for the development of thunderstorms.

Figure 1 shows distributions of the rainfall accumulation on undisturbed days. The areas in which the total rainfall accumulation exceeds 1000 mm are principally located on the western side of the Snow Mountain Range (SMR) and the CMR (Fig. 1a). The analysis about diurnal rainfall cycle was shown in Fig 1b. The hourly averaged rainfall increased significantly in afternoon hours (after 1200 LST and before 21 LST) and reached a maximum during 1500–1600 LST. The diurnal variation implied that the heavier precipitation confined

on the slopes of the SMR and CMR in the absence of large-scale weather systems were subjectively correlated with the afternoon thunderstorms (Lin and Kuo 1996; Chen et al. 2001).

3. Characteristics of thunderstorms

a. Temporal variations

The distributions of reflectivity (> 40 dBZ) frequencies and cloud-to-ground (CG) lightning frequencies from 1200 to 2100 LST on undisturbed days both present that two local maximum frequency areas were confined in the mountain-slope regions and were approximately parallel to the SMR and CMR (not shown), which were potentially coincident with those areas with plenty rainfall amounts as shown in Fig. 1a.

Evolutions of reflectivity (> 40 dBZ) frequencies during 1400–1700 LST on undisturbed days are shown in Fig. 2. At 1400 LST (Fig. 2a), there were four regions (shown in Fig. 2b) with relatively high frequencies adjacent to the SMR and CMR. These frequencies significantly increased at 1500 LST (Fig. 2b), especially in the middle (subdomain C) and southern (subdomain S) portions of the CMR; and their frequencies were about two times the magnitude of those in northern Taiwan (subdomains N and E). At 1600 LST (Fig. 2c), the frequencies in the subdomains C and S merged and expanded, and the overall maximum was about 10 % in the subdomain C. After 1700 LST (Fig. 2d), the high-frequency area in northern Taiwan reduced; and by 1800 LST (not shown), this decreasing trend of reflectivity (> 40 dBZ) frequencies was found in these all subdomains.

b. Hovmöller diagram over the mountain slopes

The Hovmöller diagram (e.g., Carbone et al. 2002) of reflectivity (> 40 dBZ) frequencies and CG lightning frequencies in four subdomains (N, C, S; and E in Fig. 2b, only show subdomain N and C here) were averaged along and across the ridges of the SMR or the CMR (henceforth referred to as parallel and perpendicular components), and the frequency averages were plotted with respect to time (Fig. 3). The perpendicular component of the subdomain N (Fig. 3a) showed the frequency of > 2.0 % started at 1300–1400 LST near the averaged height of 300 m on the windward slope of the SMR and reached a maximum frequency of about 3.5 % at 1500–1600 LST. For the parallel component (Fig. 3a), the spatial frequency distribution revealed a wide zone along the orientation of the SMR. Both components presented that the duration of frequency of > 2.0 % was 3–4 hours, which was between 1300 and 1700 LST.

Spatial distribution of the perpendicular component in the subdomain C (Fig. 3c), the zone of frequency > 2.0 % was confined at the averaged height of 400 m on the windward slope of the CMR. The frequency > 2.0 % started at 1400–1500 LST and reached a maximum frequency about 6.5 % at 1500–1600 LST, which was one hour later than in the subdomain N. The parallel component displayed the spatial frequency distribution

along the orientation of the CMR. Both components presented that the period of frequency > 2.0 % was during 1400–1900 LST, and the duration was about 4–5 hours, which was one hour longer than in the subdomain N.

Although the CG lightning distribution was slightly scattered and the frequencies were relatively lower (0.1–0.2 %) than those of the reflectivity, the local maximum regions were highly related (Fig. 3b and d). All the climatology Hovmöller diagrams of reflectivity and lightning (Fig. 3) show that thunderstorms principally occurred over the mountain slopes and concentrated during the afternoon hours. The spatial and temporal variations in both reflectivity > 40 dBZ and lightning appeared that the storm movement was largely affected by the orientations of the SMR and CMR. These results generally agree with the finding of Roe and Baker (2006) who argued that the orographic geometry strongly influences airflow patterns which, in turn, spatial distributions of heavy rainfall.

c. Movement of storms

To be consistent with the reflectivity climatology, a reflectivity threshold of 40 dBZ was used to define storm cells by The Storm Cell Identification and Tracking (SCIT) (Johnson et al. 1998). During 1200–2100 LST, storm-cell movement in the subdomains N, C, and S, the dominant movement of storm cells was northeastward (32 %), northward (~ 20 %) and northeastward (~ 21 %), and northward (~ 20 %), respectively. They were largely parallel to the orientations of the mountains. The results indicated that the topography may have considerable impact on not only the development but also the movement of afternoon thunderstorm.

d. Composite vertical structures

The vertical structures of the afternoon thunderstorms were analyzed using the climatological contoured frequency by altitude diagrams (CFADs), which is the frequency distributions of any given reflectivity range at a given altitude (Yuter and Houze 1995). In this study, CFADs were computed in convective regions that were roughly defined as areas within 10 km radius of the storm-cell locations (Steiner et al. 1995) identified by the SCIT algorithm.

RCWF data were analyzed for thunderstorms in northern Taiwan and RCCG data for central to southern Taiwan. The convective CFADs during 1200–2100 LST on undisturbed days are shown in Fig. 4. The CFADs from RCWF and RCCG radar showed that below 6 km, the near-vertically aligned contours with a strong gradient were seen within the range of frequency of between 45 and 55 dBZ. This vertically aligned convective profiles were different from the brightband maximum at the freezing level in the stratiform profile, as documented in Steiner et al. (1995). The CFADs also showed a higher frequency (> 18 %, Fig. 4b) in southern Taiwan than that in northern Taiwan (~ 16 %, Fig. 4a),

indicating stronger afternoon thunderstorms in southern Taiwan than in the north. In addition, the vertical extent of 40 dBZ can reach to an altitude higher than 10 km MSL, which typically corresponds to a temperature of lower than -20°C in warm seasons over Taiwan area. It's implied that the great majority of storms could potentially produce CG lightning (e.g., Hondl and Eilts 1994), as shown in Fig. 3.

4. Preconvective environments

To investigate preconvective atmospheric conditions for the local thunderstorms in Taiwan, the undisturbed days (identified in section 2) were separated into TSA and non-TSA days according to radar reflectivity and lightning data. Then sounding and surface observations for TSA and non-TSA days are analyzed and compared to investigate the distinctions of prethunderstorm atmospheric conditions.

a. Definition of thunderstorm days

As the interpretation explained in section 3a and 3d, reflectivity values > 40 dBZ and CG lightning can reasonably describe the spatial and temporal distributions of thunderstorms (e.g., Steiger et al. 2007). Accordingly, a TSA day is defined with reflectivity greater than 40 dBZ where CG lightning occurred between 1200–2100 LST on undisturbed days in this study. There are 89 TSA days identified in northwestern Taiwan, 145 days in central Taiwan, 94 days in southern Taiwan, and only 49 days in northeastern Taiwan.

b. Mean sounding profiles

Panchiao sounding launched at approximately 0800 LST (0000 UTC) was selected to study the large-scale preconvective environments of thunderstorms occurred in northern Taiwan. The temperature (T) and dew-point temperature (Td) profiles were averaged for all undisturbed days (277 days), TSA days (89 days) and non-TSA days (188 days), respectively, and then differences between the averaged profiles from all undisturbed days versus TSA and non-TSA days were computed.

On TSA days, the near-surface layer was found to be relatively warmer ($+0.5^{\circ}\text{C}$ in mean T) and moister ($+1.0^{\circ}\text{C}$ in mean Td) than the average of all undisturbed days. On non-TSA days, the near-surface layer was relatively cooler (-0.2°C in mean T) and drier (-0.5°C in mean Td) than the average of all undisturbed days. In the lower to middle troposphere, non-TSA days were drier than TSA days, with the difference of $1.5\text{--}3.5^{\circ}\text{C}$ in mean Td especially around 700–600 hPa layer. The results in the current study generally agree with the argument in Craven et al. (2002), who found that lifting the most unstable parcel in the lower atmosphere had the strongest relationship with convective activity.

Jou (1994) addressed that the convective system developed along the mean low-to-middle tropospheric wind in northern Taiwan. The histograms of wind directions between an altitude of 0–3 km and 3–6 km for

each sounding on TSA and non-TSA days show that the most frequent wind direction was the southwesterly wind between an altitude of 0 and 6 km on TSA days (not shown), whereas the southwesterly component between an altitude of 3 and 6 km on non-TSA days was indistinct (not shown). The pronounced southwesterly wind on TSA days may likely contribute to the most frequent of northeastward movement of storm cells as described in section 3c and could provide relatively warmer and moister environments to trigger moist convection and promote air parcels to overcome entrainment at the mid-troposphere layer (Zehnder et al. 2006).

c. Diurnal variations

Diurnal variations in average surface winds on TSA and non-TSA days revealed a convergence during 1000–1400 LST (not shown), which was caused by the northwestern flow from the Danshui valley and northeastern flow from the Keelung River valley in northern Taiwan. On non-TSA days, the wind directions in Taipei Basin comprehended more northeasterly component than on TSA days. The results are consistent with the study in undisturbed environments over Taiwan area (e.g., Kerns et al. 2009). The surface mean T from station Danshui (46690), Taipei (46692), and Keelung (46694) were generally higher on TSA days than on non-TSA days with a difference of about $0.5\text{--}1.5^{\circ}\text{C}$ warmer before afternoon thunderstorms occurred (not shown). Surface mean Td at Danshui and Keelung showed the differences with a daily mean value of approximately $1\text{--}2^{\circ}\text{C}$ between TSA and non-TSA days during morning and early afternoon (not shown).

In central Taiwan, in addition to the western flow from Chiayi County, there was a slightly southern component to the diurnal average surface winds on TSA days from Tainan County during 1000–1400 LST (not shown), in contrast to the slightly northern component to the diurnal average surface winds on non-TSA days. The resultant convergence on TSA days may have provided favorable conditions for thunderstorms over the western slope of the CMR. The surface mean T were generally $0.5\text{--}1^{\circ}\text{C}$ warmer on TSA days than on non-TSA days at station Yungkang (46742), Chiayi (46748), and Chigu (46778) during morning and early afternoon (not shown). In addition, pronounced higher surface mean Td at the stations on TSA days were about $0.5\text{--}1.5^{\circ}\text{C}$ higher than on non-TSA days during morning and early afternoon (not shown). In northern and central Taiwan, the relatively warmer T and more moisture could provide a favorable environment for the initiation and development of moist convection as discussed in Craven et al. (2002).

5. Conclusion

The reflectivity and CG lightning climatology both indicated that the maximum thunderstorm frequencies in different parts of Taiwan were all during 1500–1600 LST and high thunderstorm frequencies primarily

confined over the mountain slopes and approximately parallel to the ridges of the SMR and CMR. Storm activity strongly depended on geographic features while more thunderstorm activity was found in central to southern Taiwan than in northern and eastern Taiwan. Although Thunderstorms occurred earlier in northern Taiwan than in the other parts of Taiwan, the durations of thunderstorm activity in central to southern Taiwan were longer than in northern Taiwan.

The preconvective environments associated with the occurrences of afternoon thunderstorms observed from sounding showed the mean T and Td in near-surface layer were relatively warmer and moister on TSA days than non-TSA days. In lower to middle troposphere, the T profile on non-TSA days was also drier than TSA days. The wind directions in the 0–3 and 3–6 km layers also indicated that relatively humid southwesterly flows potentially provided more favorable conditions with less entrainment during the development of afternoon thunderstorms.

Diurnal variations in northern Taiwan, the northwestern flow from the Danshui valley and northeastern flow from the Keelung River valley converged during mornings and early afternoons. Moreover, in central Taiwan, the convergence of surface wind caused by the western flow from Chiayi County and slightly southern flow component from Tainan County. Diurnal variations of northern and central Taiwan in surface mean T and Td pronounced they were generally warmer and higher, respectively, on TSA days than on non-TSA days before afternoon thunderstorm occurred. These preconvective features may be integrated in real-time tools via fuzzy logic type of approaches (e.g., Berenguer et al. 2006) to improve operational predictions of afternoon thunderstorms in Taiwan.

Reference

- Akaeda, K., J. Reisner, and D. Parsons, 1995: The role of mesoscale and topographically induced circulations initiating a flash flood observed during the TAMEX project. *Mon. Wea. Rev.*, **123**, 1720–1739.
- Berenguer, M., D. Sempere-Torres, C. Corral, and R. Sánchez-Diezma, 2006: A fuzzy logic technique for identifying nonprecipitating echoes in radar scans. *J. Atmos. Oceanic Technol.*, **23**, 1157–1180.
- Carbone, R. E., J. D. Tuttle, D. A. Ahijevych, and S. B. Trier, 2002: Inferences of predictability associated with warm season precipitation episodes. *J. Atmos. Sci.*, **59**, 2033–2056.
- Chen, G. T.-J., H. C. Chou, T. C. Chang, and C. S. Liu, 2001: Frontal and non-frontal convection over northern Taiwan in mei-yu season (in Chinese with English abstract). *Atmos. Sci.*, **29**, 37–52.
- Chen, Y. L., and J. Li, 1995: Characteristics of surface airflow and pressure patterns over the island of Taiwan during TAMEX. *Mon. Wea. Rev.*, **123**, 695–716.
- Craven, J., R. Jewell, and H. Brook, 2002: Comparison between observed convective cloud-base heights and lifting condensation level for two different lifted parcels. *Wea. Forecasting*, **17**, 885–890.
- Hondl, K. D., and M. D. Eilts, 1994: Doppler radar signatures of developing thunderstorms and their potential to indicate the onset of cloud-to-ground lightning. *Mon. Wea. Rev.*, **122**, 1818–1836.
- Johnson, J. T., P. L. Mackeen, A. Witt, E. D. Mitchell, G. J. Stumpf, M. D. Eilts, and K. W. Thomas, 1998: The storm cell identification and tracking algorithm: An enhanced WSR-88D algorithm. *Wea. Forecasting*, **13**, 263–276.
- Jou, B. J.-D., 1994: Mountain-originated mesoscale precipitation system in northern Taiwan: A case study 21 June 1991. *T. A. O.*, **5**, 169–197.
- Kerns, B. W. J., Y. L. Chen, and M. Y. Chang, 2009: The diurnal cycle of winds, rain, and clouds over Taiwan during the mei-yu, summer, and autumn rainfall regimes. *Mon. Wea. Rev.* (in press).
- Lin, S. M., and H. C. Kuo, 1996: A study of summertime afternoon convection in southern Taiwan during 1994. (in Chinese with English abstract). *Atmos. Sci.*, **24**, 249–280.
- Roe, G. H., and M. B. Baker, 2006: Microphysical and geometrical controls on the pattern of orographic precipitation. *J. Atmos. Sci.*, **63**, 861–880.
- Saxen, T. R., C. K. Mueller, T. T. Warner, M. Steiner, E. E. Ellison, E. W. Hatfield, T. L. Betancourt, S. M. Dettling, and N. A. Oien, 2008: The operational mesogamma-scale analysis and forecast system of the U.S. army test and evaluation command. Part IV: The White Sands Missile Range auto-nowcast system. *J. Appl. Meteor. Climatol.*, **47**, 1123–1139.
- Steiger, S. M., R. E. Orville, and L. D. Carey, 2007: Total lightning signatures of thunderstorm intensity over North Texas. Part I: Supercells. *Mon. Wea. Rev.*, **135**, 3281–3302.
- Steiner, M., R. A. Houze, Jr., and S. E. Yuter, 1995: Climatological characterization of three-dimensional storm structure from operational radar and rain gauge data. *J. Appl. Meteor.*, **34**, 1978–2007.
- Wilson, J. W., and W. E. Schreiber, 1986: Initiation of convective storms at radar-observed boundary-layer convergence lines. *Mon. Wea. Rev.*, **114**, 2516–2536.
- Yuter, S. E., and R. A. Houze, Jr., 1995: Three-dimensional kinematic and microphysical evolution of Florida cumulonimbus. Part II: Frequency distributions of vertical velocity, reflectivity, and differential reflectivity. *Mon. Wea. Rev.*, **123**, 1941–1963.
- Zehnder, J. A., L. Zhang, D. Hansford, A. Radzan, N. Selover, and C. M. Brown, 2006: Using digital cloud photogrammetry to characterize the onset and transition from shallow to deep convection over orography. *Mon. Wea. Rev.*, **134**, 2527–2546.

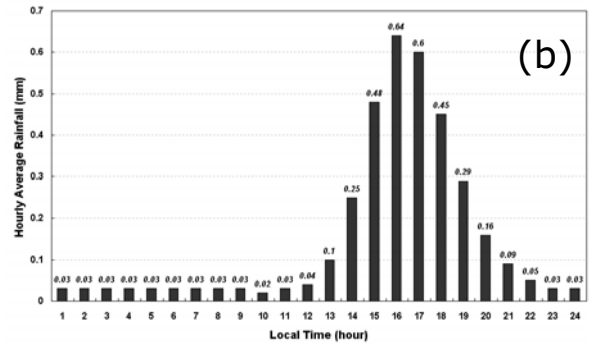
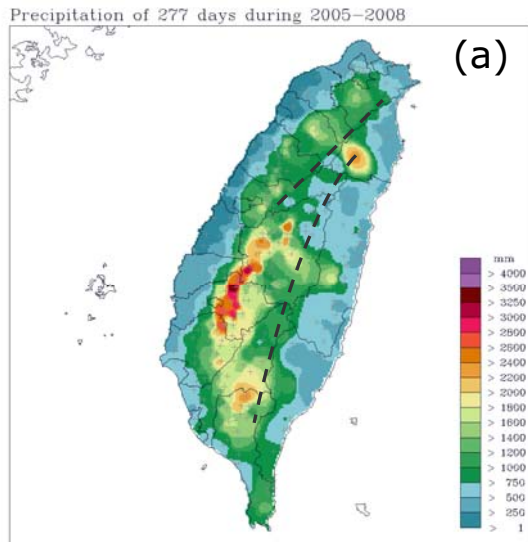


FIG. 1. (a) Distribution of rainfall (mm) on undisturbed days during the warm seasons in 2005–2008. (b) Hourly average rainfall (mm) for all rain gauges. The dashed lines indicate the crest lines of SMR and CMR ranges.

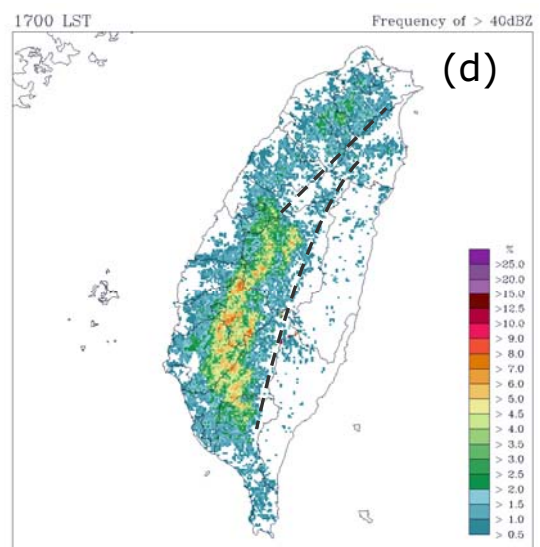
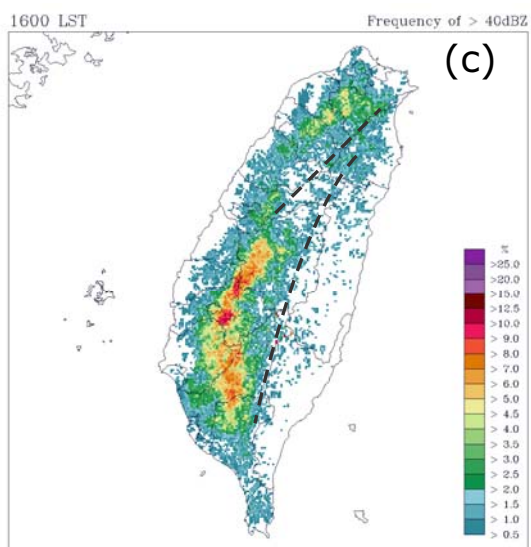
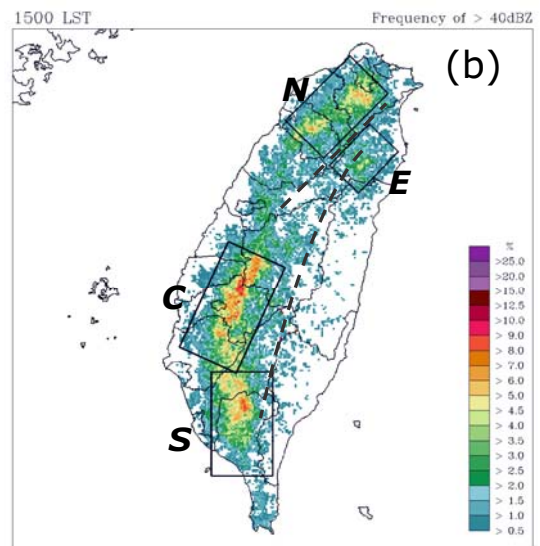
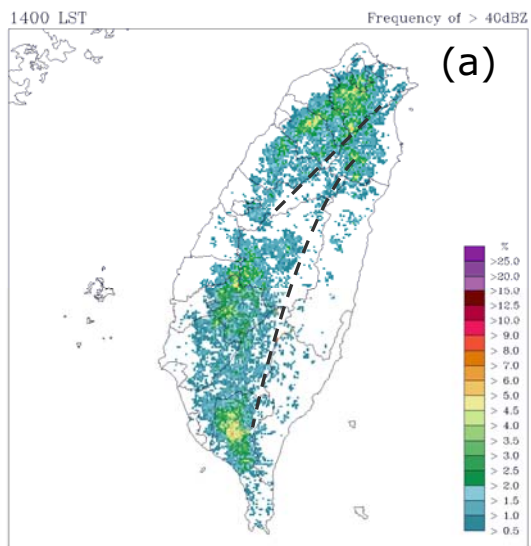


FIG. 2. Frequency of occurrence (%) for reflectivity > 40 dBZ at (a) 1400, (b) 1500, (c) 1600, and (d) 1700 LST on undisturbed days. The four inset boxes in (b) indicate the subdomains for calculating the Hovmöller diagrams in Figs. 3.

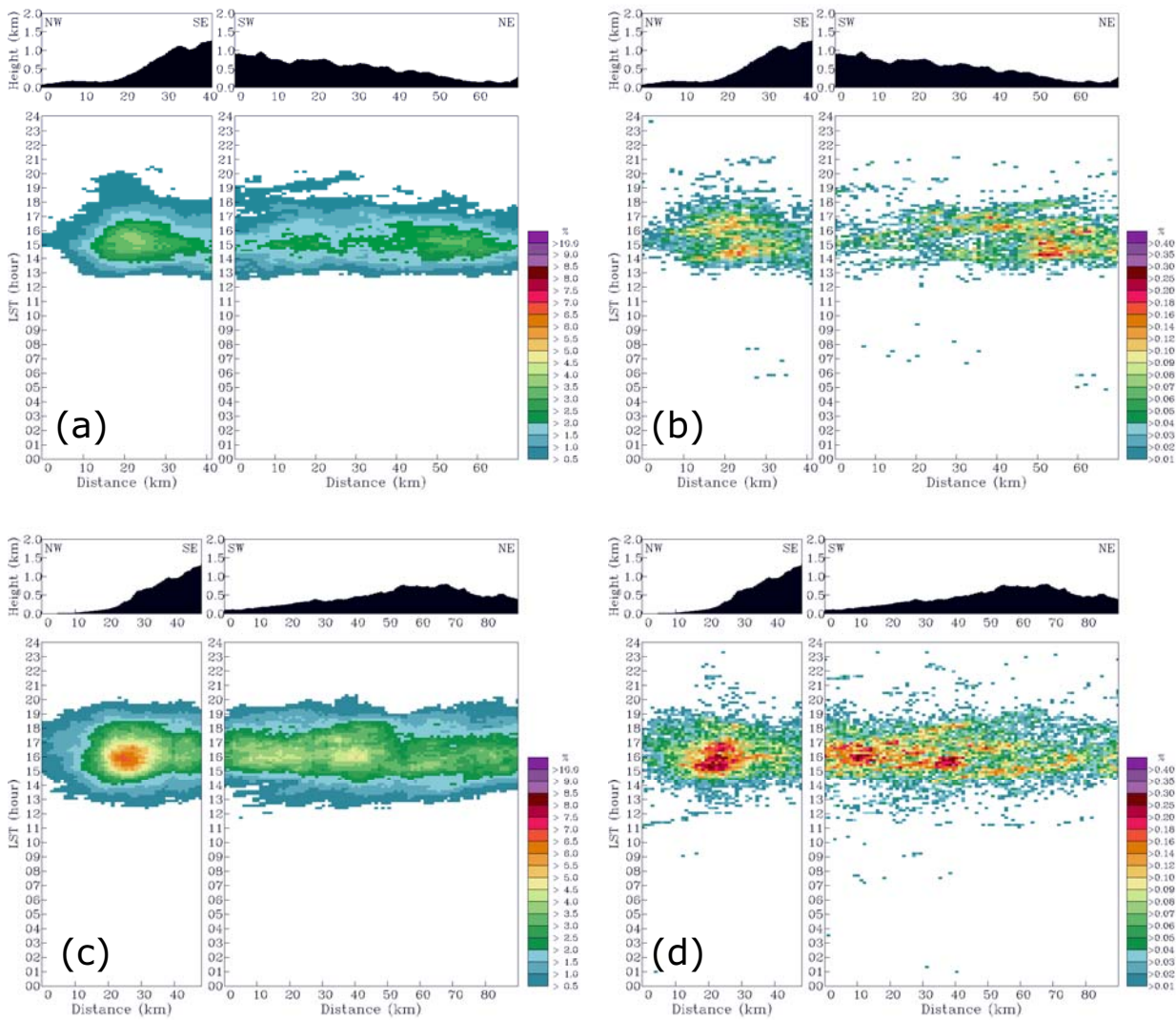


FIG. 3. Hovmöller diagrams of the frequency of occurrence (%) of reflectivity > 40 dBZ on undisturbed days: (a) is for the subdomain N; and (c) is for the subdomain C. Similarly, (b) and (d) are for the CG lightning in the subdomains N and C, respectively. In each Hovmöller diagram, the frequency in the left (or right) panel is averaged with across (or along) the long side of the subdomain as indicated in Fig. 2b. The average topographic profile is also indicated at the top of each figure.

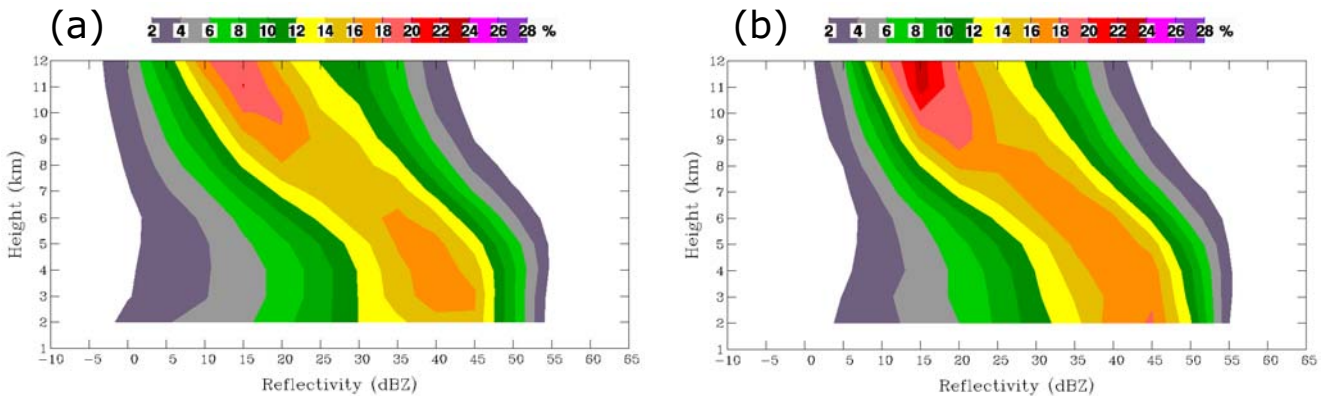


FIG. 4. Climatological contoured frequency by altitude diagrams (CFADs) of radar reflectivity for (a) RCWF data collected at 6-minute intervals and (b) RCCG data collected at 10-min intervals during 1200–2100 LST on undisturbed days. The CFAD bin size is 5 dBZ and is shaded with colors at intervals of 2 % of data per dBZ per kilometer.